Carbon nanotube arrays as monolayer nanoscale membrane for enhanced desalination

Tianzhen Wang, Haifeng Jiang*, Xingyu Shao, Junxian Pei, Huai Zheng, Xuejiao Hu*

Key Laboratory of Hydraulic Machinery Transients (Wuhan University), Ministry of Education, School of Power and Mechanical Engineering, Wuhan University, Wuhan, Hubei 430072, China, emails: hfjiang@whu.edu.cn (H. Jiang), xjhu@whu.edu.cn (X. Hu), 2015102080027@whu.edu.cn (T. Wang), 2020202080034@whu.edu.cn (X. Shao), 2012302650048@whu.edu.cn (J. Pei), huai_zheng@whu.edu.cn (H. Zheng)

ABSTRACT

Carbon nanotubes (CNTs) have attracted considerable attention due to their extraordinary properties, which makes them very attractive in various applications such as desalination. The single-layer parallel arranged carbon nanotubes (SPACNTs) can form slits that allow water to pass along the outer wall of the CNTs while blocking salt ions. In this work, the water flow rate and desalination of SPACNTs were studied. Through molecular dynamics simulations, the filtration efficiency of water and ions in channels with varying radius (from 0.5 to 3.0 nm) of CNTs and slit size (from 0.7 to 1.5 nm) was studied. When the slit between CNTs is 0.7 nm with a 3 nm radius, the maximum water flow rate of 1,200 L/(m² h bar) and the salt rejection close to 100% are shown. This work provides some theoretical guidance for the study of CNT membranes for desalination.

Keywords: Carbon nanotubes; Desalination; Water permeability; Molecular dynamics

1. Introduction

Reliable water resources on the earth are very limited, and the challenge of global water shortage has attracted increasing attention. Although 70% of the earth's surface is water, non-saline water only accounts for less than 3% [1]. Among the various forms of water on the earth, seawater accounts for 97.47% of the total, with reserves of approximately 1.35 billion km³. Not only that, but about 70% of the world's population lives within 70 km of the sea according to statistics. Such a vast distribution of resources makes seawater considered the most promising source of freshwater [2]. Among different desalination technologies, reverse osmosis (RO) is the dominant one, with a total share of 53%, followed by multi-stage flash distillation, multi-effect distillation and electrodialysis [3–5].

With the development of membrane science and technology, the use of nanoscale membranes for the desalination of seawater to prepare freshwater is considered feasible and promising [6,7]. Studies have shown that the permeability of 2D materials such as graphene is two to five orders of magnitude higher than RO [8–10]. Because of their excellent chemical and mechanical stability, carbon nanotubes (CNTs) can be used as channels for desalination [11,12]. Studies have shown that due to the smoothness and regularity of CNTs, the transmission speed of its internal channels is several orders of magnitude faster than that of other nanoporous materials [13,14]. In the process of producing the membrane, the CNTs can be arranged vertically or in a mixed arrangement [15,16]. However, the inner diameter of CNTs must be small enough to resist salts and must be large enough to achieve the ideal water permeability [17,18]. Another way is to make water molecules pass through the channels between the CNTs instead of the inside of the CNTs to achieve the purpose of desalination. At this time, the main factors affecting salt rejection

* Corresponding authors.

and water flow rate are the spacing between CNTs and the arrangement of CNTs [19]. The larger the thickness of the membrane, the more it will hinder the water flow rate, so we always hope to reduce the thickness of the membrane to increase the water flow rate while blocking salts.

In this article, we mainly focus on single-layer parallel arranged carbon nanotubes (SPACNTs) to obtain a larger water flow rate. The channel formed between adjacent CNTs is similar to the shape of an hourglass. It has been reported that compared with the permeability of porous graphene to water, the channel in the shape of an hourglass has better water permeability [20]. So molecular dynamics (MD) simulation is used to study the resistance, desalination and configuration of water molecules to reveal the excellent desalination performance as water molecules passing through the SPACNTs.

2. Simulation details

All the MD simulations were performed with a Large-scale Atomic/Molecular Massively Parallel Simulator (LAMMPS) [21]. The Chemistry at HARvard Macromolecular Mechanics 27 (CHARMM27) force field [22] and the extended simple point-charge (SPC/E) water model [23] were used. The Lennard–Jones (LJ) parameters are summarized in Table 1. Other LJ parameters were obtained by using the Lorentz–Berthelot rules [24]. The van der Waals (vdW)

Table 1
Potential parameters of atoms [26]

Atom	σ (Å)	ε (kcal/mol)	q (e)
C (C–C)	3.851	0.105	0
O (H_2O)	3.166	0.155	–0.834
H (H_2O)	0.000	0.000	+0.417
Na	2.430	0.0469	+1
Cl	4.045	0.146	–1

coupling was calculated with a cutoff of 12 Å. The Verlet algorithm is used to integrate Newton's equations of motion. Before applying pressure to the top graphene, the system was thermal balanced using the canonical ensemble (NVT ensemble). The Nose−Hoover thermostat is used to maintain a constant temperature. The particle–particle–particle–mesh method was used to treat long-range electrostatic interactions [25]. The simulations were conducted in the NVT ensemble at T = 298 K with a time step of 1 fs. At the first part of the simulation, atmospheric pressure was applied to both pistons in the opposite directions to ensure the density of water is equal to 998 kg/m³, the relaxation process of the system is 1 ns.

The model discussed in this paper is shown in Fig. 1. The SPACNTs are arranged in parallel and can be regarded as a single-layer membrane composed of CNTs. For the convenience of simulation calculation and discussion, the CNTs are not staggered or arranged in multilayers. The staggered arrangement of CNTs or arrangement of multi-layered CNTs is more complicated to study. Based on the principle of simplicity to complexity, this article mainly discusses the SPACNTs. Relatively complex issues are reserved for follow-up research.

The specific model used in the simulation is shown in Fig. S1. Two graphene pistons are used to confine the salt solution and apply a pressure difference across the membrane. The upper graphene piston is applied with the downward pressure of 200 MPa, and the lower graphene piston is applied with an upward pressure of 0.1 MPa. Applying a larger pressure difference can also simulate a more severe situation, because the salt rejection rate decreases as the pressure difference increase [10,27]. The length of the CNT is 3.3 nm. The salt concentration of the feed solution is set to 0.6 mol/L, which is similar to the salt concentration of seawater. Because periodic boundary conditions can be used in the simulation, the SPACNTs model can be simplified to a single-channel model as shown in Fig. S1 in the supplementary material. The single-channel model is formed by placing two semicircular
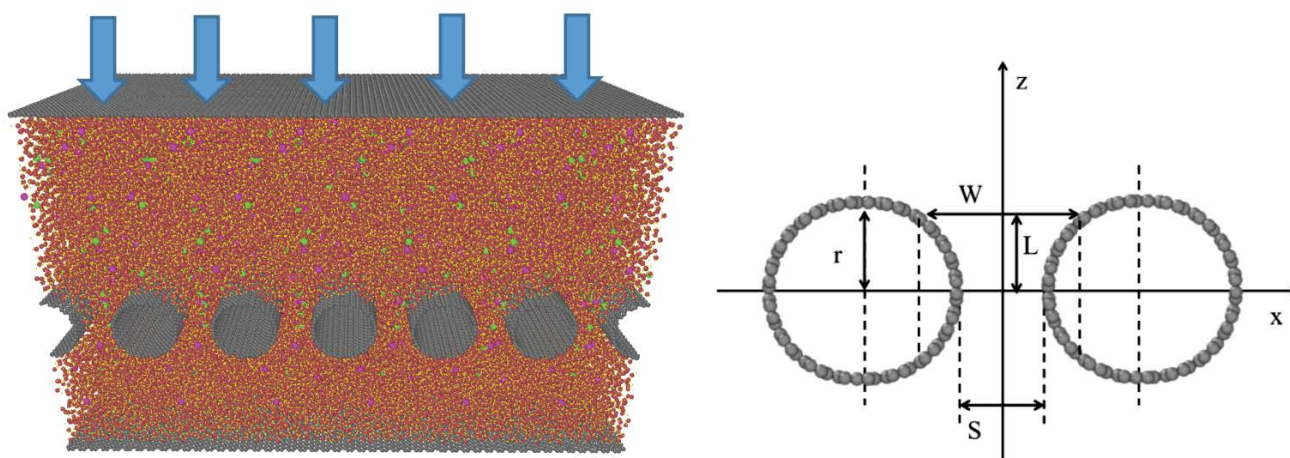
Fig. 1. Desalination process using horizontal array of CNTs. Under the pressure of the topmost graphene piston, water flows from top to bottom through a monolayer of CNTs (left). The figure on the right is the annotation of the relevant dimension parameters of the studied model. Black represents carbon atoms, red represents oxygen atoms, yellow represents hydrogen atoms, rose red represents sodium ions, and green represents chloride ions.

CNTs facing each other. The resistance and water flow rate of a single nanochannel are discussed below, and then the water flow rate of SPACNTs is discussed.

3. Theory model

Under macro conditions, a continuous medium model is generally used to describe the flow of fluids. However, in the case of micro-nano scales (such as the fluid flow between graphene oxide layers), the particle nature of the fluid becomes impossible to ignore. The ratio of the average free path length λ of the particles to the characteristic size L of the object is defined as the Knudsen number Kn. The Knudsen number is often used to divide whether the flowing medium is continuous:

Kn < 10^{-3} Continuum

10^{-3}< Kn < 10^{-1} Temperature jump and velocity slip

10^{-1}< Kn < 10^{1} Transition

10^{1}< Kn   Free-molecule

When water molecules flow through the nanochannel, Kn is about 0.1, so the fluid flow is in the velocity slip regime [28,29]. According to the former literatures [30–34], the entrance resistance of our model in Fig. 1 can be estimated as:

$$R_e = \frac{3.8\mu}{\left(S+2r\right)^3} \tag{1}$$

where μ is the viscosity of water. S is the slit size between the nanotubes. r is the radius of the nanotubes. Similar to the entrance resistance, the outlet resistance can be estimated as:

$$R_0 = \frac{3.8\mu}{S^3} \tag{2}$$

In the literature mentioned above, considering the slipped boundary, the resistance of parallel plates is shown as:

$$R_p = \frac{\Delta P}{Q} = \frac{12\mu L_p}{BW^3\left(1+\frac{6\zeta}{W}\right)} \tag{3}$$

In the above equation, ζ is the slip length; L_p is the length of the plate; B is the length of the CNTs in the y-direction; W is the different values of the slit size of carbon atoms on two adjacent CNTs varying with axis z, which can be represented by Eq. (4):

$$W = S + 2\left(r - \sqrt{r^2 - L^2}\right) \tag{4}$$

where L is the ordinate value of the carbon atom on the CNT; r is the radius of the CNTs.

It can be assumed that the hourglass channel is composed of an infinite number of parallel plates. The resistance of each tiny plate resistance can be written as follows:

$$dR_t = \frac{12\mu}{BW^3\left(1+\frac{6\zeta}{W}\right)}dL \tag{5}$$

Then the resistance formula of the hourglass channel is obtained by integrating the resistance of all the tiny plates along the CNT wall:

$$R_t = \int_0^{L_t} \frac{12\mu}{BW^3\left(1+\frac{6\zeta}{W}\right)}dL \tag{6}$$

The resistances at the entrance, inner and outlet of the channel all had impacts on the flow. All those resistances should be added to the total resistance. The three factors were considered in a series connection form, as shown in Eq. (7):

$$Q = \frac{\Delta P}{R_e + R_t + R_0} \tag{7}$$

Salt rejection is calculated as follows:

$$R = \left(1 - \frac{c_p}{c_f}\right) \times 100\% \tag{8}$$

where c_p and c_f are the concentrations of the permeate and feed solution, respectively.

Assuming that the width of SPACNTs is M. For comparison, suppose there are two types of CNTs with different radii, r_1 and r_2. The numbers of the two types of CNTs contained in the membranes are N_1 and N_2, respectively. The calculation formula is shown in Eq. (9). S is the distance between adjacent CNTs.

$$N_1 = \frac{M}{2r_1 + S} \quad N_2 = \frac{M}{2r_2 + S} \tag{9}$$

The total resistance is composed of the resistance of all single channels in parallel. In the cross-section of the entire channel through which water flows, the total resistances R_1 and R_2 of the two types of CNT membranes mentioned above are shown by Eq. (10). C_1 and C_2 are the resistance of a single channel formed by two CNTs with different radii.

$$\frac{1}{R_1} = N_1\frac{1}{C_1}, \quad \frac{1}{R_2} = N_2\frac{1}{C_2} \tag{10}$$

4. Results and discussion

MD simulation was carried out to initially study the single channel of SPACNTs. The radius of CNT considered was 0.5, 1.0, 2.0, and 3.0 nm and the slit size between

CNTs was 0.7, 0.9, 1.1, 1.3, and 1.5 nm. It can be seen from Eq. (2) that there is an inversely proportional relationship between slit resistance and slit size. So as the slit size gets larger, the water flow increases accordingly which is shown in Fig. 2. When the radius of CNTs is less than 2.0 nm, the water flow rate shows a downward trend. The water flow rate reaches the maximum value while the radius of CNTs is 2.0 nm, and as the CNTs radius increases to 3.0 nm, the water flow rate remains basically unchanged. The influence of the change of CNTs radius on the water flow rate will be discussed later.

Using Eqs. (1)–(7), the effect of different CNT radii and different slip coefficients on the water flow rate are illustrated in Fig. S2. In Fig. S2, when the slip coefficient is close to 0, the CNT radius increases, and the water flow rate goes through a process of increasing first and then decreasing. This trend is inconsistent with the trend of MD simulation results. The study has reported that the slip length of fluid flow in CNTs is several nanometers [35]. Here the slip coefficient of a single channel is assumed to be about 5 nm. Fig. 2b is the water flow rate change under different CNT radius when the channel slip coefficient is 5 nm. It can be seen from the figure that under the same radius, the water flow rate increases as the slit size. Under the same slit size, and the water flow rate experiences a trend of increasing first and then basically unchanged. This trend is in good agreement with the trend of MD simulation results. Actually, the slip coefficient of the single channel of SPACNTs is unknown. Because the slip coefficient is related to the diffuse reflection coefficient, the relationship between the diffuse reflection coefficient and the surface curvature of the CNTs needs to be studied to determine the slip coefficient. This will be the next research topic and will not be discussed in this paper.

To better explain the influence of the channel on the water flow, it is necessary to study the spatial configuration of the water inside the channel. By studying the orientation of water molecules relative to the channel the reason why the water flow rate tends to decrease as the radius decrease will further explain. Fig. S3 shows the definition of the two angles, α and θ, where α is related to the direction of the dipole moment of water molecules, and θ is related to the direction of the normal vector of the water molecule plane. Fig. 3 displays the distribution of θ under different slit sizes and radii, it can be seen that as the radius of CNTs increases, θ will be more near 90°. This phenomenon is more obvious with a bigger radius. In other words, water is more likely to be in the configuration shown in Fig. S4 and as the radius of CNTs increases, the water molecules become more ordered. It has been reported that the ordered structure of water molecules formed in parallel channels enables water molecules to pass through the channels quickly [36,37]. This work is consistent with the results of previous literature. The larger radius makes the water molecules more orderly, and the flow rate is bigger. For the same outlet size, the inlet of SPACNTs is wider than that of parallel channels, making it easier for water molecules to transition from a disordered configuration to an ordered one. In addition, it can be imagined that when the radius of CNTs becomes larger, the exit of the channel will be closer to the parallel channel, and the water molecules will be more orderly. Therefore, when the radius of CNTs becomes larger, the flow rate increases. However, with the increase of CNTs radius, the water molecules are subjected to greater resistance along the path, which can explain why the flow rate does not further increase with the increase of CNTs radius.

Figs. 4 and 5 list the θ and α distributions of water molecules in the channels with slit sizes of 0.7 and 1.5 nm and radii of 0.5 and 3.0 nm. The angular frequency distribution diagrams in other cases can be referred to Figs. S5–S9. Different from Fig. 3, it can be seen from Fig. 4 that changing the slit size or radius of the CNTs has a less obvious influence on the distribution of α. The configuration of water molecules passing through the channel is more concentrated in the vicinity of α = 90°, which means that the
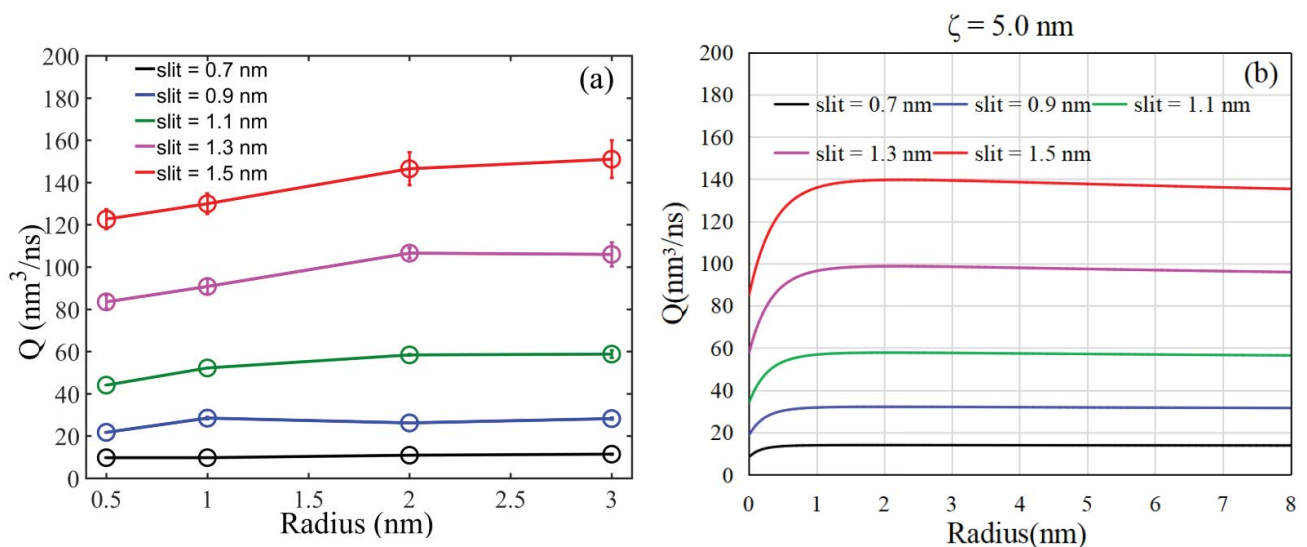
Fig. 2. (a) The water flow rate of the single channel of SPACNTs under different radii and different slit size. (b) The theoretically calculated water flow rate.
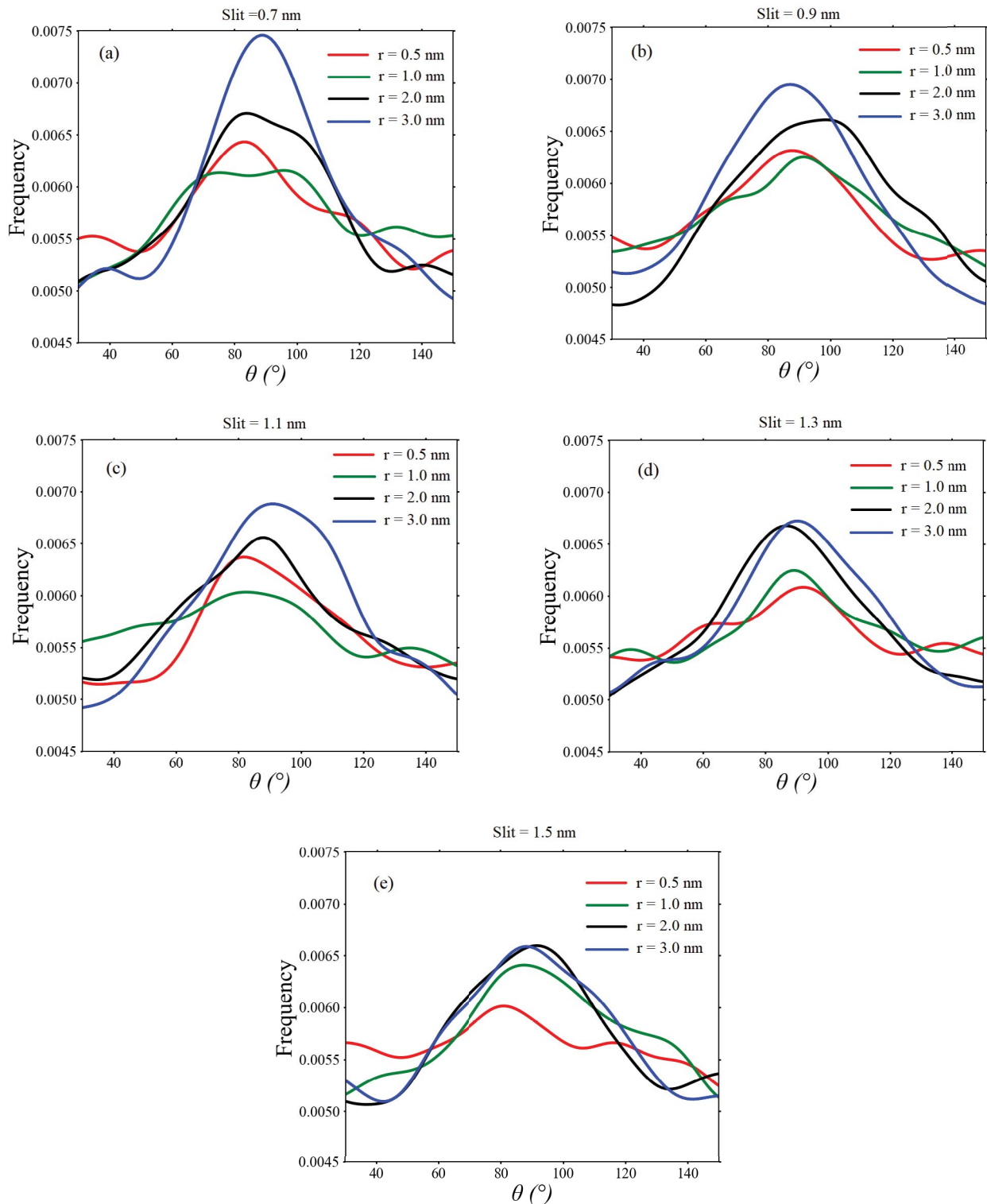
Fig. 3. Distribution of θ under different slit sizes and radii.

water molecules pass through the channel more in a configuration with a dipole moment perpendicular to the *xy* plane. The change in the slit size or radius of the CNTs will affect the freedom of water molecules to rotate around their own dipole moment, but will not affect the directionality of the water molecule dipole moment. When the slit size of CNTs decreases or the radius becomes bigger, the freedom of water molecules to rotate around their own dipole moment is restricted, and the water molecules are bound by the channel. It can be seen from Fig. 5 that the highlighted

(a) slit = 0.7 nm   r = 0.5 nm

(b) slit = 0.7 nm   r = 3.0 nm

(c) slit = 1.5 nm   r = 0.5 nm

(d) slit = 1.5 nm   r = 3.0 nm
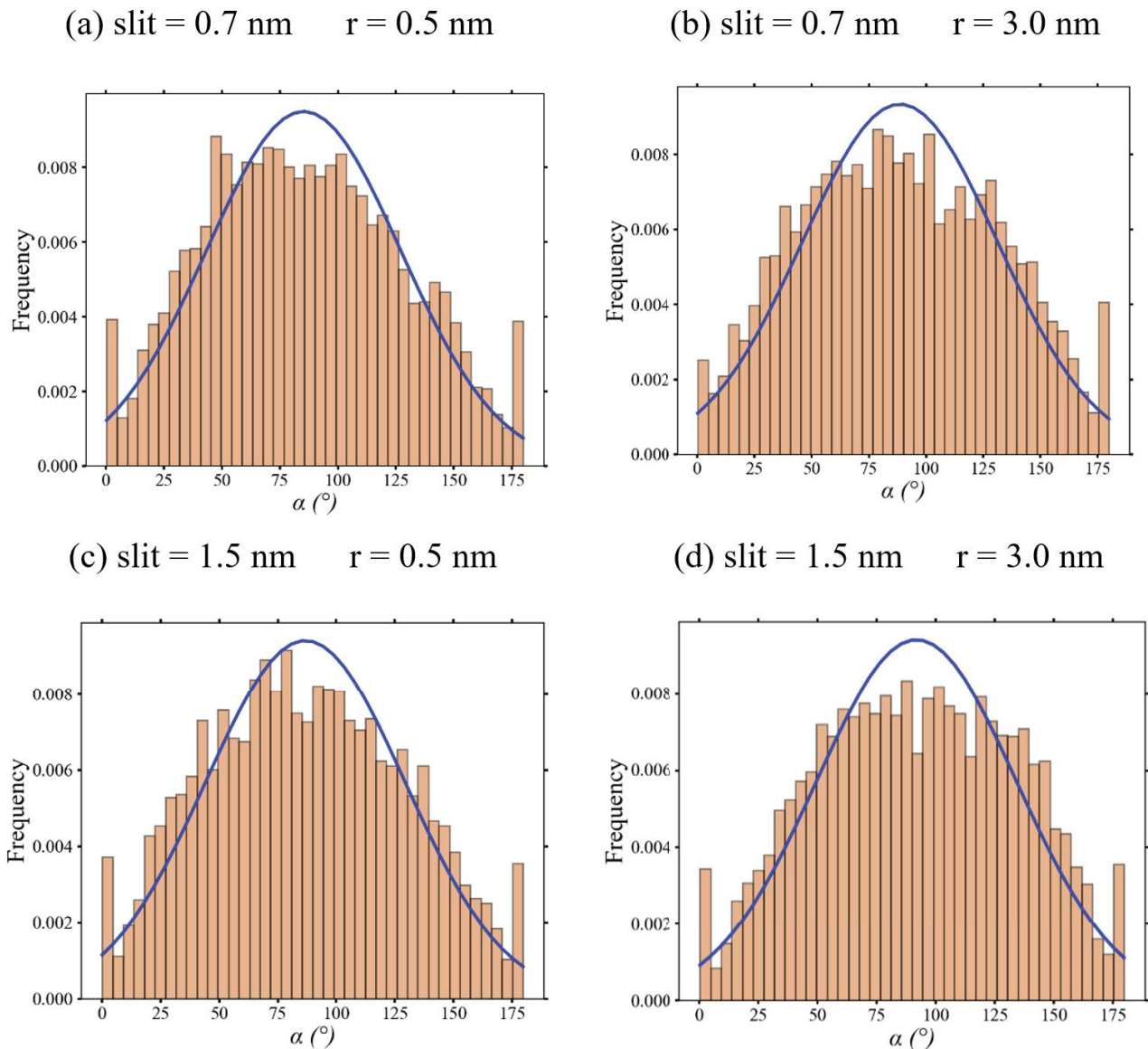
Fig. 4. Distribution of α. To make more obvious, four figures are chosen from Figs. S5–S9 for comparison. The slits between CNTs and the radii of CNTs are marked above the figures.

area become more concentrated with a smaller distance between CNTs or the bigger radius, meaning that the distribution of angles becomes more concentrated.

It can be seen from Fig. 6 that the salt rejection rate is obviously affected by the change of the slit size, but not by the change of the radius. When the slit size is 0.7 nm, the salt rejection rate is basically close to 100%. In other cases, the salt rejection rate is lower. According to Koneshan et al. [38], the hydration radius of sodium ions is about 0.32 nm. When the hydration diameter of sodium ions is close to the narrowest part of the nanochannel (0.7 nm), the permeability of ions in the channel is significantly inhibited.

The above discussion is for a single nanochannel in SPACNTs. In the following, the water flow rate of SPACNTs was studied using Eqs. (9) and (10). For the sake of comparison, CNTs with two radii of r_1 and r_2 were used to form two

kinds of SPACNTs membranes. As shown in Fig. 2, it can be known that the ratio Q_2/Q_1 of the water flow of the single nanochannel of SPACNTs of r_1 = 0.5 nm and r_2 = 2.0 nm is ~1.2. Under the same pressure difference, the resistance ratio C_2/C_1 of these two single nanochannels is ~0.83. When S = 1.5 nm, N_1/N_2 = 2.2 can be calculated by Eq. (9), so R_2/R_1 = ~1.83 can be obtained by Eq. (10). Therefore, the water flow rate of SPACNTs with r_1 = 0.5 nm will be ~1.83 times the water flow rate with r_2 = 2.0 nm. If r_1 = 2.0 nm and r_2 = 5.0 nm, when S = 1.5 nm, N_1/N_2 = ~2, C_2/C_1 is ~1.0. At this time, R_2/R_1 = ~2 can be calculated by Eq. (10). Therefore, the water flow rate of SPACNTs with r_1 = 2.0 nm will be ~2 times the water flow rate with r_2 = 5.0 nm.

As shown in Fig. 7, the MD simulation results of this work are compared with the data in the previous literature. Here is to compare the water flow rate of the model with a

(a) slit = 0.7 nm   r = 0.5 nm   (b) slit = 0.7 nm   r = 3.0 nm

(c) slit = 1.5 nm   r = 0.5 nm   (d) slit = 1.5 nm   r = 3.0 nm
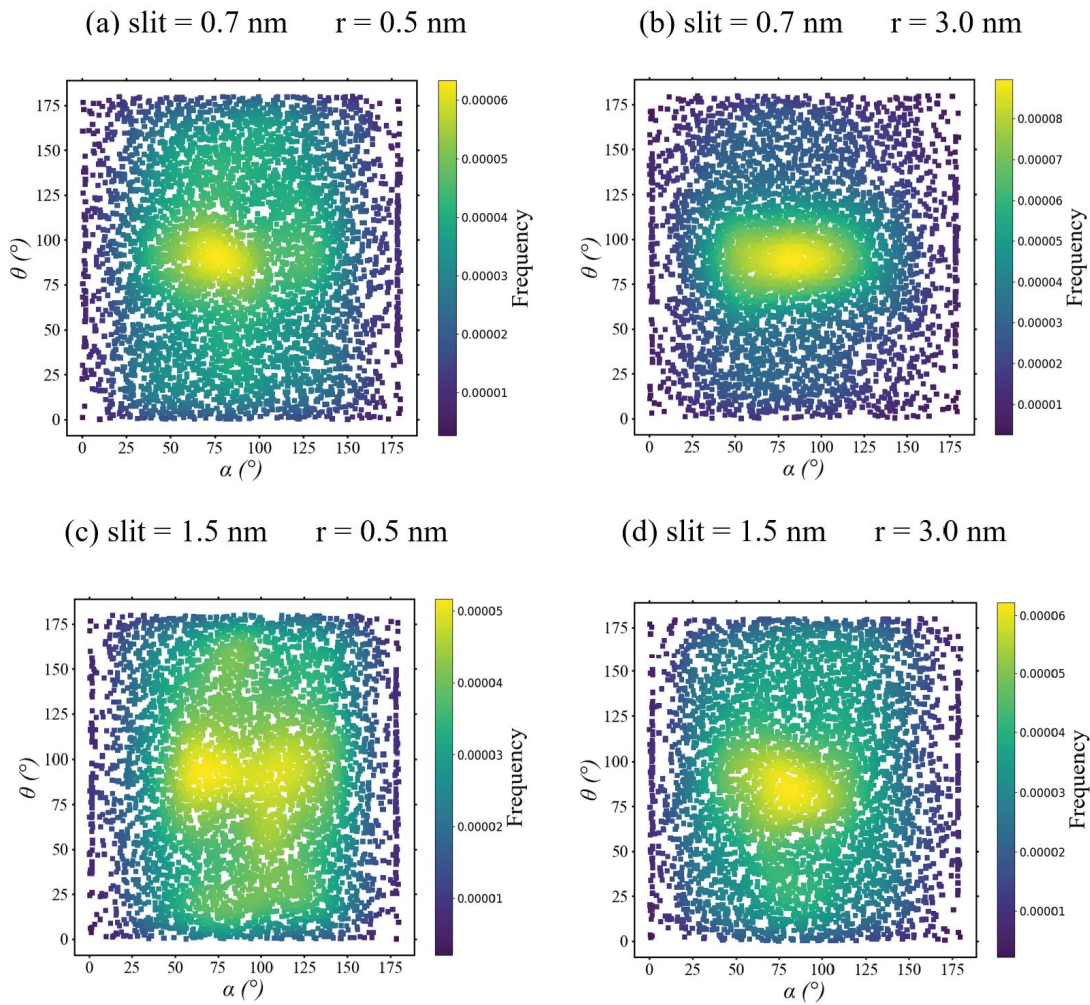
Fig. 5. Bivariate joint distribution of θ and α. To make more obvious, four figures are chosen from Figs. S5–S9 for comparison. The slits between CNTs and the radii of CNTs are marked above the figures.
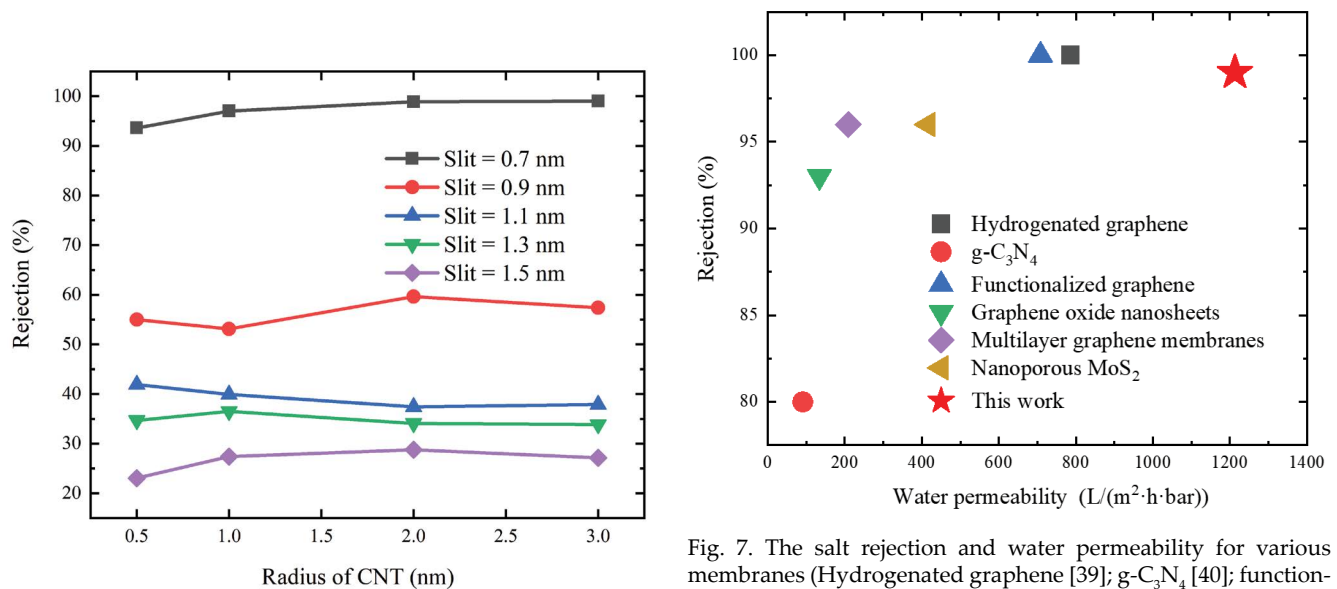
Fig. 6. Salt rejection with different radii under different slits.

Fig. 7. The salt rejection and water permeability for various membranes (Hydrogenated graphene [39]; g-C$_3$N$_4$ [40]; functionalized graphene [41]; graphene oxide nanosheets [42]; multilayer graphene membrane [43]; nanoporous MoS$_2$ [44].)

radius of 3.0 nm and a slit of 0.7 nm with other data. The picture contains different materials and structures. There are C_3N_4, MoS_2, graphene oxide nanosheets, graphene with functional groups and multilayer graphene structures. Through comparison, it is found that the water flow rate of the SPACNTs used in this article is at a relatively high level. In the case of a high water flow rate, the salt rejection rate can be maintained above 95%.

5. Conclusion

In this paper, MD simulation is used to study the water flow rate and desalination effect of SPACNTS. Through simulation studies, it is found that for a single channel in SPACNTS, the water flow rate increases as the CNT slit size increases, but exactly the opposite for the salt rejection rate. On the other hand, the water flow rate gradually increases with the radius of CNTs become larger and when CNTs radius increases to 2~3 nm, the maximum flow appears. It depends on the configuration of the water molecules in the channel. However, for SPACNTs, the water flow rate with small radii of CNTs is higher than that with large radii. Even if the SPACNTs are still in the computational design stage, we hope that the relevant results shown in this work can inspire further work to make this concept a reality. Further experiments are needed to verify the mechanical stability of the membrane and the effects of fouling and concentration polarization.

References

[1] P.H. Gleick, Water in Crisis: A Guide to the World's Fresh Water Resources, Oxford University Press, New York, 1993.

[2] M.A. Shannon, P.W. Bohn, M. Elimelech, J.G. Georgiadis, B.J. Mariñas, A.M. Mayes, Science and technology for water purification in the coming decades, Nature, 452 (2008) 301–310.

[3] D. Xevgenos, K. Moustakas, D. Malamis, M. Loizidou, An overview on desalination & sustainability: renewable energy-driven desalination and brine management, Desal. Water. Treat., 57 (2014) 2304–2314.

[4] D. Xevgenos, M. Marcou, V. Louca, E. Avramidi, G. Ioannou, M. Argyrou, P. Stavrou, M. Mortou, F.C. Küpper, Aspects of environmental impacts of seawater desalination: Cyprus as a case study, Desal. Water Treat., 211 (2021) 15–30.

[5] S. Herrera-León, C. Cruz, A. Kraslawski, L.A. Cisternas, Current situation and major challenges of desalination in Chile, Desal. Water Treat., 171 (2019) 93–104.

[6] P.R. Kidambi, D. Jang, J.C. Idrobo, M.S.H. Boutilier, L. Wang, J. Kong, R. Karnik, Nanoporous atomically thin graphene membranes for desalting and dialysis applications, Adv. Mater., 29 (2017) 1700277, doi: 10.1002/adma.201700277.

[7] A. Kalra, S. Garde, G. Hummer, Osmotic water transport through carbon nanotube membranes, Proc. Natl. Acad. Sci. U.S.A., 100 (2003) 10175–10180.

[8] E.Y.M. Ang, T.Y. Ng, J. Yeo, Z. Liu, K.R. Geethalakshmi, Free-standing graphene slit membrane for enhanced desalination, Carbon, 110 (2016) 350–355.

[9] D. Cohen-Tanugi, J.C. Grossman, Nanoporous graphene as a reverse osmosis membrane: recent insights from theory and simulation, Desalination, 366 (2015) 59–70.

[10] M. Heiranian, A.B. Farimani, N.R. Aluru, Water desalination with a single-layer MoS_2 nanopore, Nat. Commun., 6 (2015) 8616, doi: 10.1038/ncomms9616.

[11] R.H. Tunuguntl, R.Y. Henley, Y.C. Yao, T.A. Pham, M. Wanunu, A. No, Enhanced water permeability and tunable ion selectivity in subnanometer carbon nanotube porins, Science, 357 (2017) 792–796.

[12] E. Secchi, S. Marbach, A. Niguès, D. Stein, A. Siria, L. Bocquet, Massive radius-dependent flow slippage in carbon nanotubes, Nature, 537 (2016) 210–213.

[13] J.K. Holt, Carbon nanotubes and nanofluidic transport, Adv. Mater., 21 (2009) 3542–3550.

[14] M. Majumder, N. Chopra, R. Andrews, B.J. Hinds, Nanoscale hydrodynamics: enhanced flow in carbon nanotubes, Nature, 438 (2005) 44, doi: 10.1038/438044a.

[15] C.H. Ahn, Y. Baek, C. Lee, S.O. Kim, S. Kim, S. Lee, S.-H. Kim, S.S. Bae, J. Park, J. Yoon, Carbon nanotube-based membranes: Fabrication and application to desalination, J. Ind. Eng. Chem., 18 (2012) 1551–1559.

[16] S. Trivedi, K. Alameh, Effect of vertically aligned carbon nanotube density on the water flux and salt rejection in desalination membranes, Springerplus, 5 (2016) 1158, doi: 10.1186/s40064-016-2783-3.

[17] R. Das, M.E. Ali, S.B.A. Hamid, S. Ramakrishna, Z.Z. Chowdhury, Carbon nanotube membranes for water purification: A bright future in water desalination, Desalination, 336 (2014) 97–109.

[18] B. Corry, Designing carbon nanotube membranes for efficient water desalination, J. Phys. Chem. B, 112 (2008) 1427–1434.

[19] E.Y.M. Ang, T.Y. Ng, J. Yeo, R. Lin, K.R. Geethalakshmi, Nanoscale fluid mechanics working principles of transverse flow carbon nanotube membrane for enhanced desalination, Int. J. Appl. Mech., 9 (2017) 1750034, doi: 10.1142/S175882511750034X.

[20] S. Gravelle, L. Joly, C. Ybert, L. Bocquet, Large permeabilities of hourglass nanopores: from hydrodynamics to single file transport, J. Chem. Phys., 141 (2014) 18C526.

[21] S. Plimpton, Fast parallel algorithms for short-range molecular dynamics, J. Comput. Phys., 117 (1995) 1–19.

[22] M. Patra, M. Karttunen, Systematic comparison of force fields for microscopic simulations of NaCl in aqueous solutions: diffusion, free energy of hydration and structural properties, J. Comput. Chem., 25 (2004) 1–13.

[23] M. Rezaei, A.R. Azimian, A.R. Pishevar, Surface charge-dependent hydrodynamic properties of an electroosmotic slip flow, Phys. Chem. Chem. Phys., 20 (2018) 30365–30375.

[24] W.F. van Gunsteren, P.K. Weiner, A.J. Wilkinson, Computer Simulation of Biomolecular Systems: Theoretical and Experimental Applications, Springer, Netherlands, 1997.

[25] R.W. Hockney, J.W. Eastwood, Computer Simulation Using Particle, CRC Press, Boca Raton, 1988.

[26] B. Hess, C. Holm, N. van der Vegt, Osmotic coefficients of atomistic NaCl (aq) force fields, J. Chem. Phys., 124 (2006) 164509, doi: doi: 10.1063/1.2185105.

[27] D. Cohen-Tanugi, J.C. Grossman, Water desalination across nanoporous graphene, Nano Lett., 12 (2012) 3602–3608.

[28] H. Liu, Y. Liu, J. Dai, Q. Cheng, An improved model of carbon nanotube conveying flow by considering comprehensive effects of Knudsen number, Microfluid. Nanofluid., 22 (2018) 66, doi: 10.1007/s10404-018-2088-7.

[29] F. Kaviani, H.R. Mirdamadi, Influence of Knudsen number on fluid viscosity for analysis of divergence in fluid conveying nano-tubes, Comp. Mater. Sci., 61 (2012) 270–277.

[30] B. Chen, H. Jiang, X. Liu, X. Hu, Molecular insight into water desalination across multilayer graphene oxide membranes, ACS Appl. Mater. Interfaces, 9 (2017) 22826–22836.

[31] B. Chen, H. Jiang, X. Liu, X. Hu, Observation and analysis of water transport through graphene oxide interlamination, J. Phys. Chem. C, 121 (2017) 1321–1328.

[32] A. Maali, T. Cohen-Bouhacina, H. Kellay, Measurement of the slip length of water flow on graphite surface, Appl. Phys. Lett., 92 (2008) 053101.

[33] N. Wei, X. Peng, Z. Xu, Breakdown of fast water transport in graphene oxides, Phys. Rev. E: Stat. Nonlinear Soft Matter Phys., 89 (2014) 012113.

[34] N. Wei, X. Peng, Z. Xu, Understanding water permeation in graphene oxide membranes, ACS Appl. Mater. Interfaces, 6 (2014) 5877–5883.

[35] E.M. Kotsalis, J.H. Walther, P. Koumoutsakos, Multiphase water flow inside carbon nanotubes, Int. J. Multiphase Flow, 30 (2004) 995–1010.

[36] M. Deng, K. Kwac, M. Li, Y. Jung, H.G. Park, Stability, molecular sieving, and ion diffusion selectivity of a lamellar membrane from two-dimensional molybdenum disulfide, Nano Lett., 17 (2017) 2342–2348.

[37] S. Jiao, Z. Xu, Non-continuum intercalated water diffusion explains fast permeation through graphene oxide membranes, ACS Nano, 11 (2017) 11152–11161.

[38] S. Koneshan, J.C. Rasaiah, R.M. Lynden-Bell, S.H. Lee, Solvent structure, dynamics, and ion mobility in aqueous solutions at 25°C, J. Chem. Phys. B, 102 (1998) 4193–4204.

[39] Y. Wang, Z. He, K.M. Gupta, Q. Shi, R. Lu, Molecular dynamics study on water desalination through functionalized nanoporous graphene, Carbon, 116 (2017) 120–127.

[40] Y. Liu, D. Xie, M. Song, L. Jiang, G. Fu, L. Liu, J. Li, Water desalination across multilayer graphitic carbon nitride membrane: insights from non-equilibrium molecular dynamics simulations, Carbon, 140 (2018) 131–138.

[41] W. Li, W. Wang, Y. Zhang, Y. Yan, P. Král, J. Zhang, Highly efficient water desalination in carbon nanocones, Carbon, 129 (2018) 374–379.

[42] M. Hu, B. Mi, Enabling graphene oxide nanosheets as water separation membranes, Environ. Sci. Technol., 47 (2013) 3715–3723.

[43] D. Cohen-Tanugi, L.C. Lin, J.C. Grossman, Multilayer nanoporous graphene membranes for water desalination, Nano Lett., 16 (2016) 1027–1033.

[44] W. Li, Y. Yang, J.K. Weber, G. Zhang, R. Zhou, Tunable, strain-controlled nanoporous MoS(2) filter for water desalination, ACS Nano, 10 (2016) 1829–1835.

Supplementary information
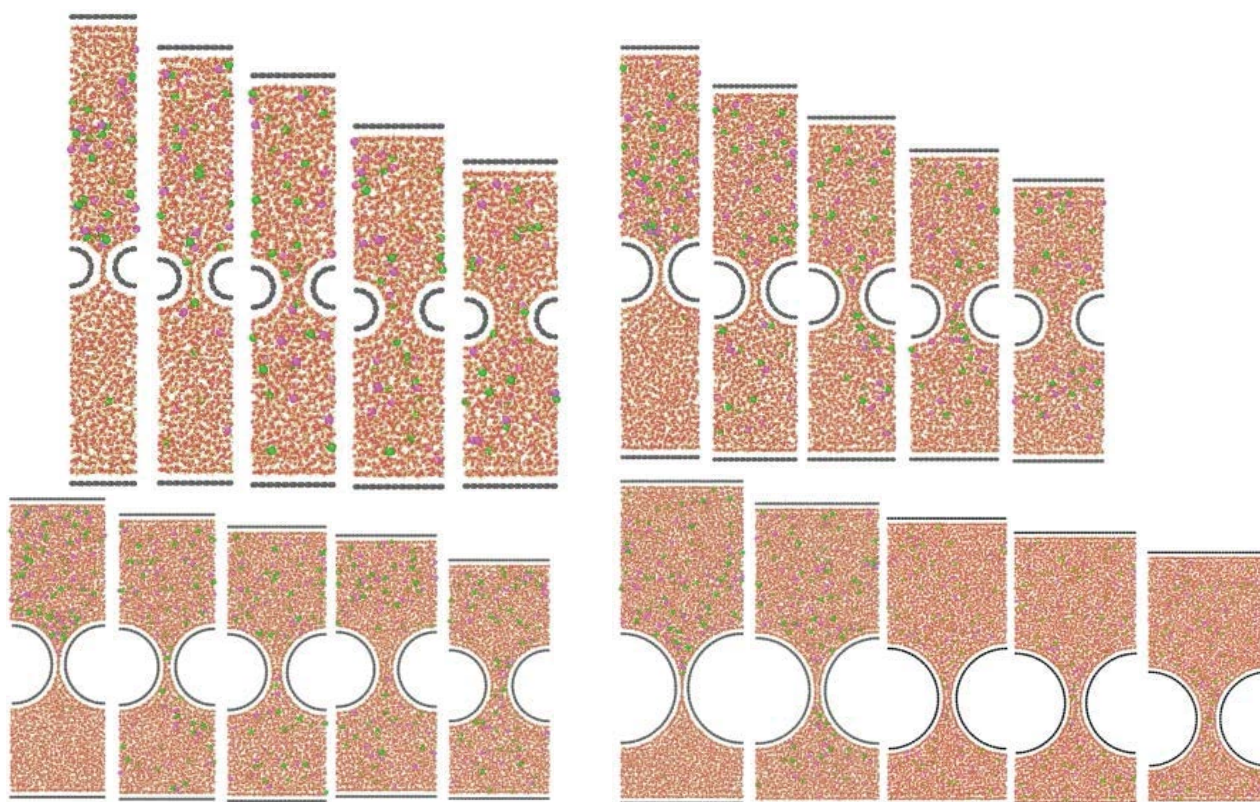
Fig. S1. The specific model used in the simulation. The radii of CNT shown in the figure are 0.5, 1.0, 2.0, and 3.0 nm from top to bottom. The slits between CNTs are 0.7, 0.9, 1.1, 1.3, and 1.5 nm from left to right. Black represents carbon atoms, red represents oxygen atoms, yellow represents hydrogen atoms, rose red represents sodium ions, and green represents chloride ions.
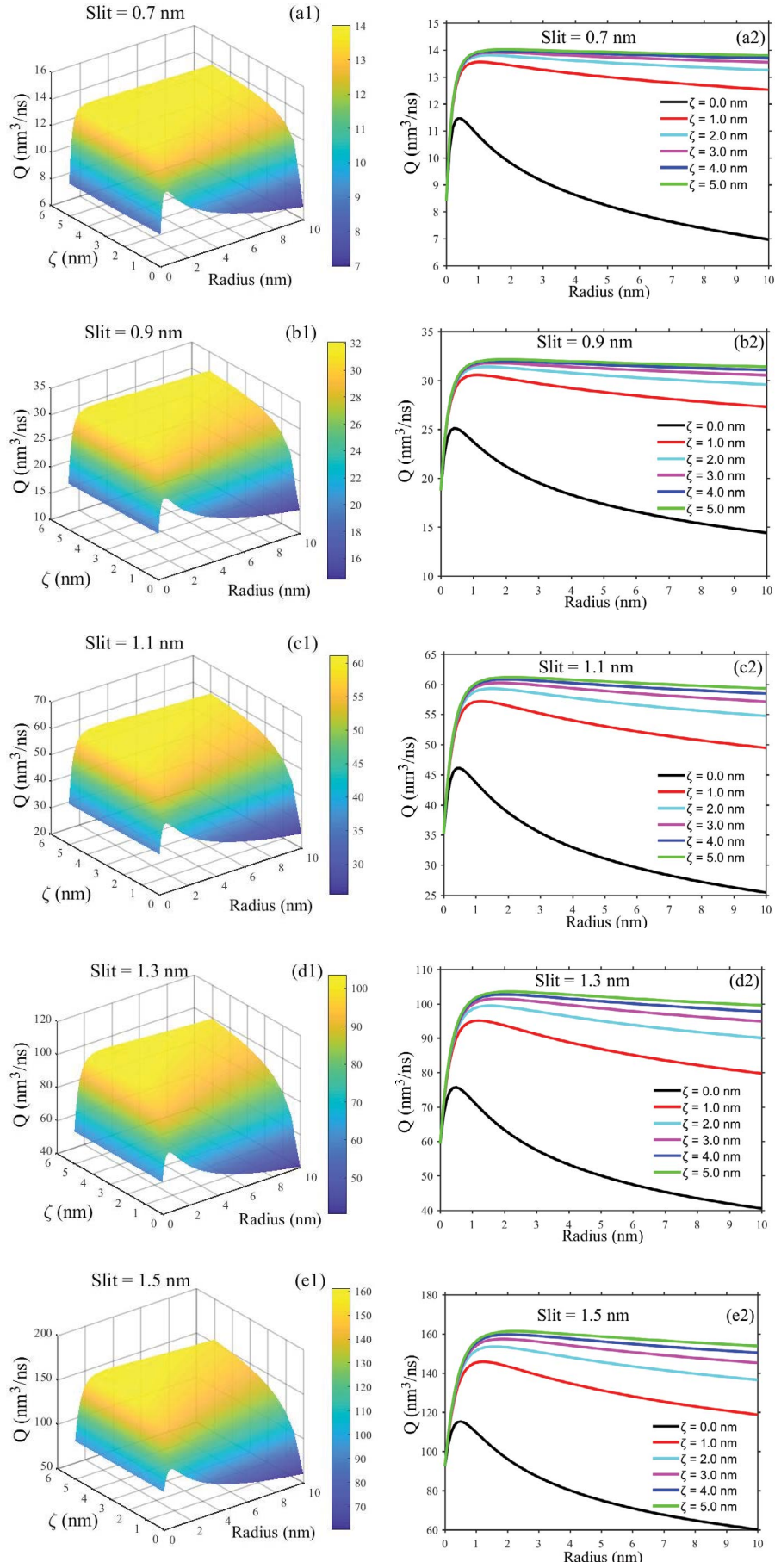
Fig. S2. The water flux of the single channel in SPACNTs under different radii and slip coefficients. (a1)–(e1) correspond to the slit size of 0.7, 0.9, 1.1, 1.3, and 1.5 nm, respectively. (a2)–(e2) correspond to the change of water flux with CNTs radius for six different slip coefficients under different slits respectively.
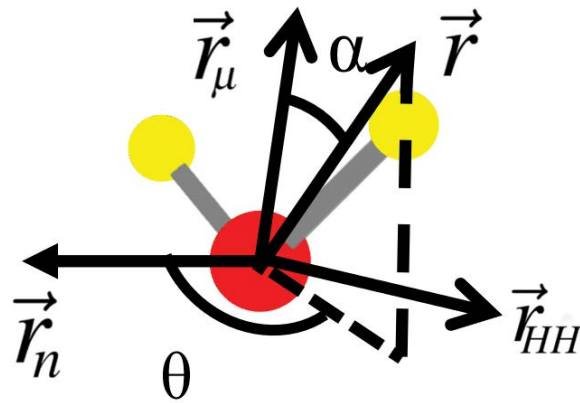
Fig. S3. The definition of θ and φ, r represents the normal vector of the yz plane, $\vec{r}_\mu$ represents the dipole moment of the water molecule, $\vec{r}_n$ is the normal vector of the water molecule plane, and $\vec{r}_{HH}$ is the vector connecting the two hydrogen atoms.
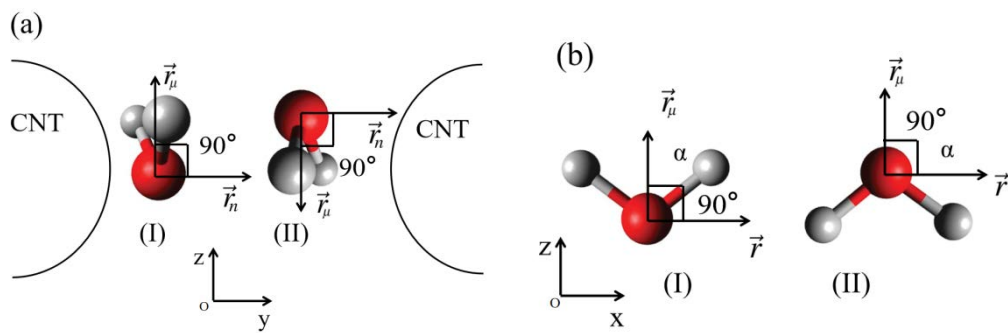
Fig. S4. The configuration of water molecules when they pass through the channels between CNTs. (a) View from a perspective parallel to the x-axis. (b) View from a perspective parallel to the y-axis.
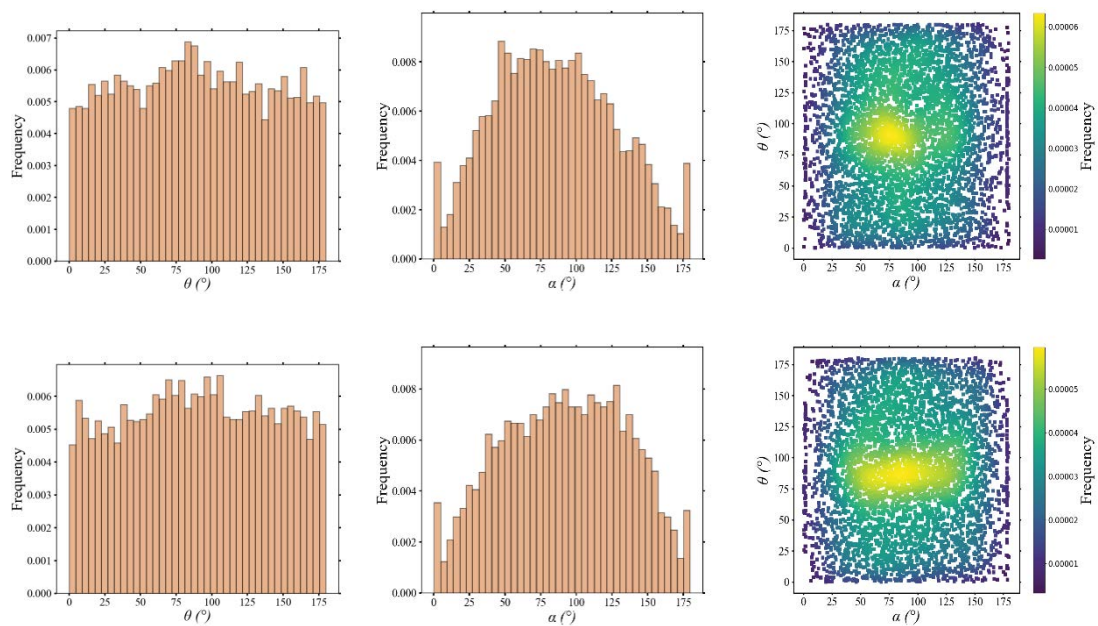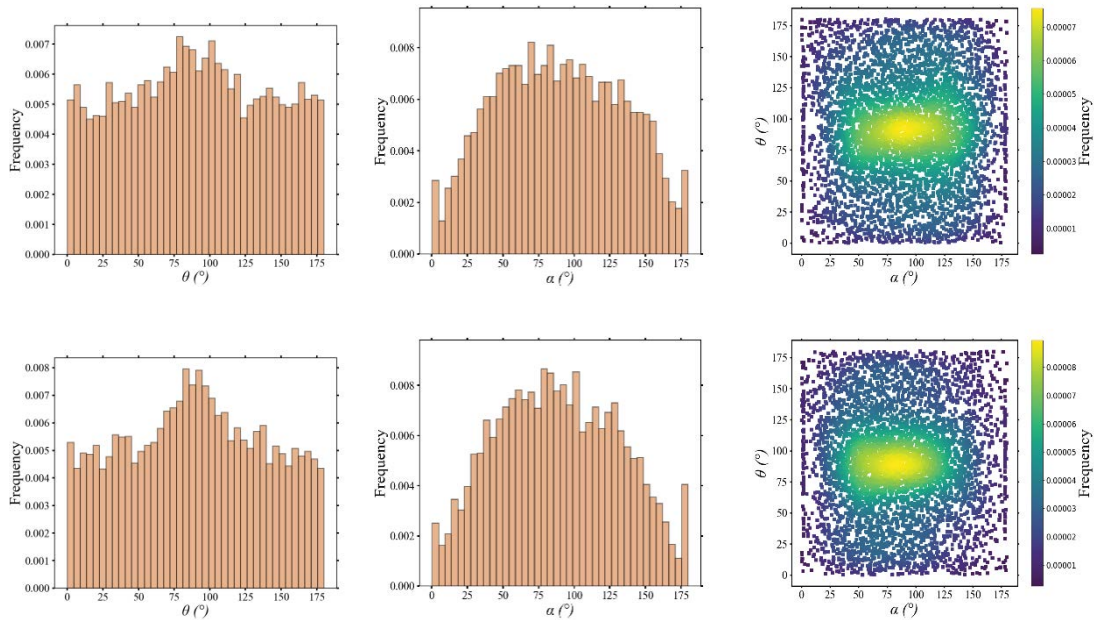
Fig. S5. The slit between CNTs is 0.7 nm, from top to bottom, each row corresponds to *r* = 0.5, 1.0, 2.0, and 3.0 nm, from left to right, each column corresponds to distribution of θ, distribution of α, bivariate joint distribution of θ and α.
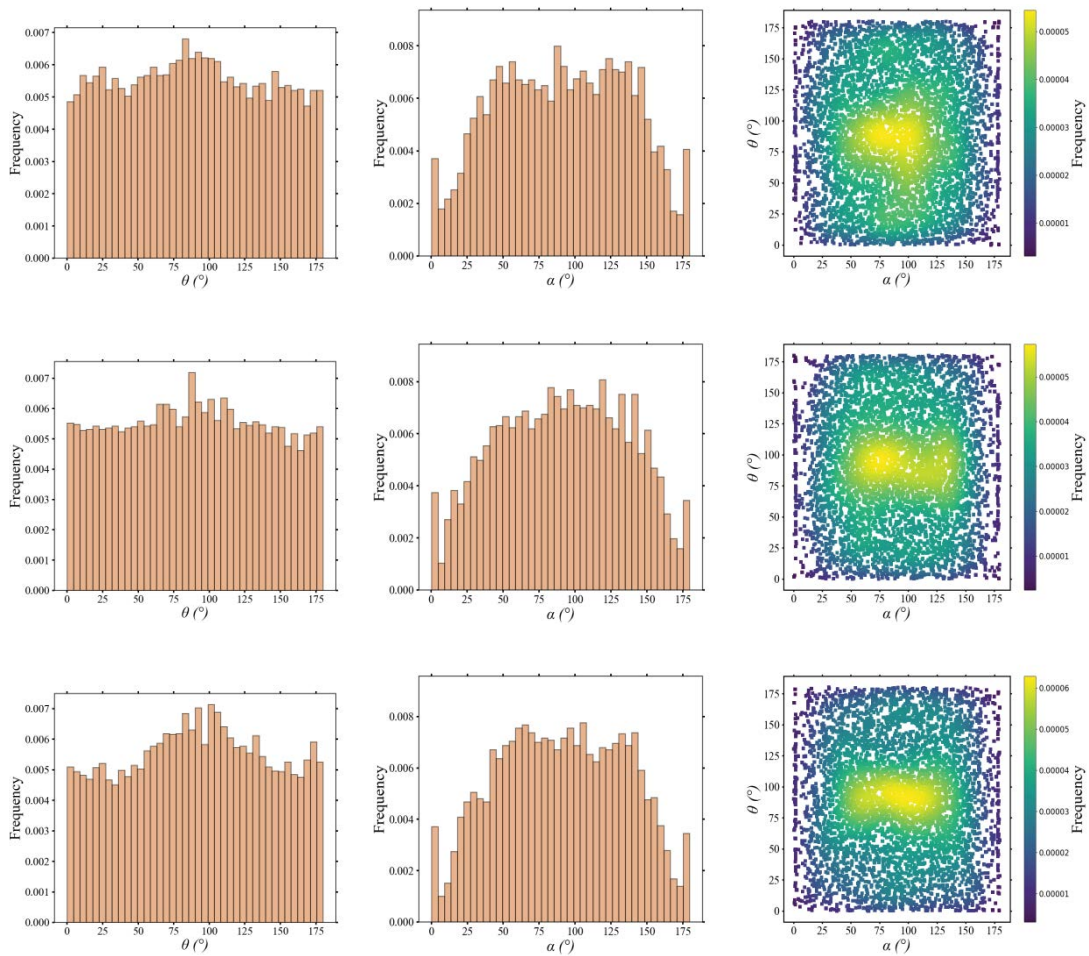
(Continued)
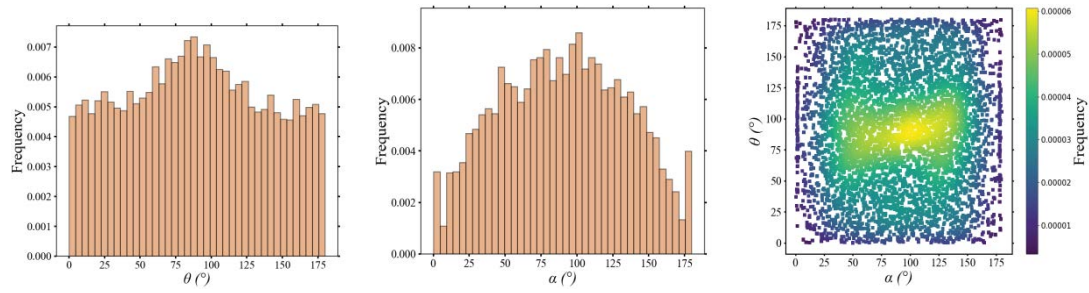
Fig. S6. The slits between CNTs is 0.9 nm, from top to bottom, each row corresponds to r = 0.5, 1.0, 2.0, and 3.0 nm, from left to right, each column corresponds to distribution of θ, distribution of α, bivariate joint distribution of θ and α.
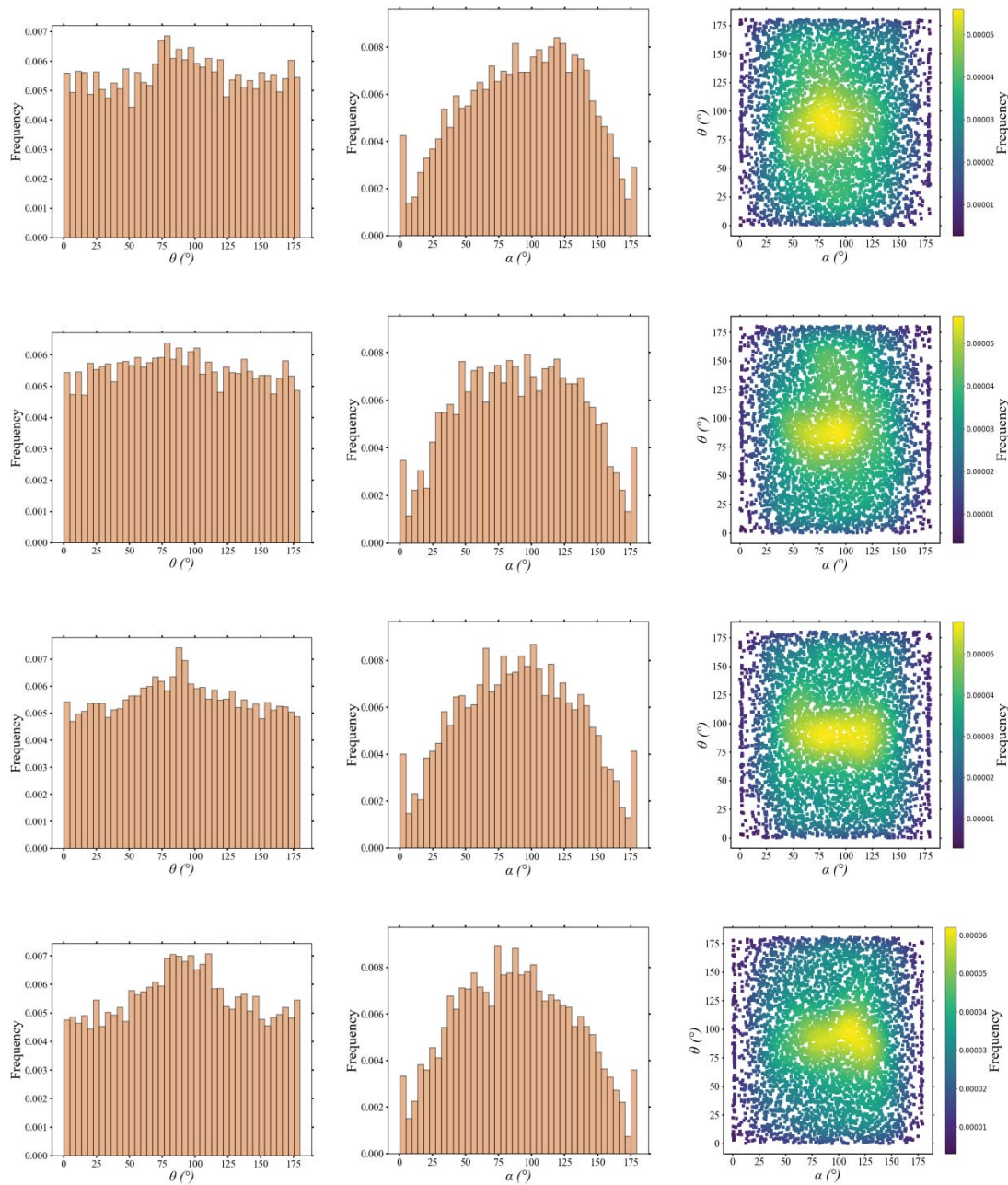
Fig. S7. The slits between CNTs is 1.1 nm, from top to bottom, each row corresponds to r = 0.5, 1.0, 2.0, and 3.0 nm, from left to right, each column corresponds to distribution of θ, distribution of α, bivariate joint distribution of θ and α.
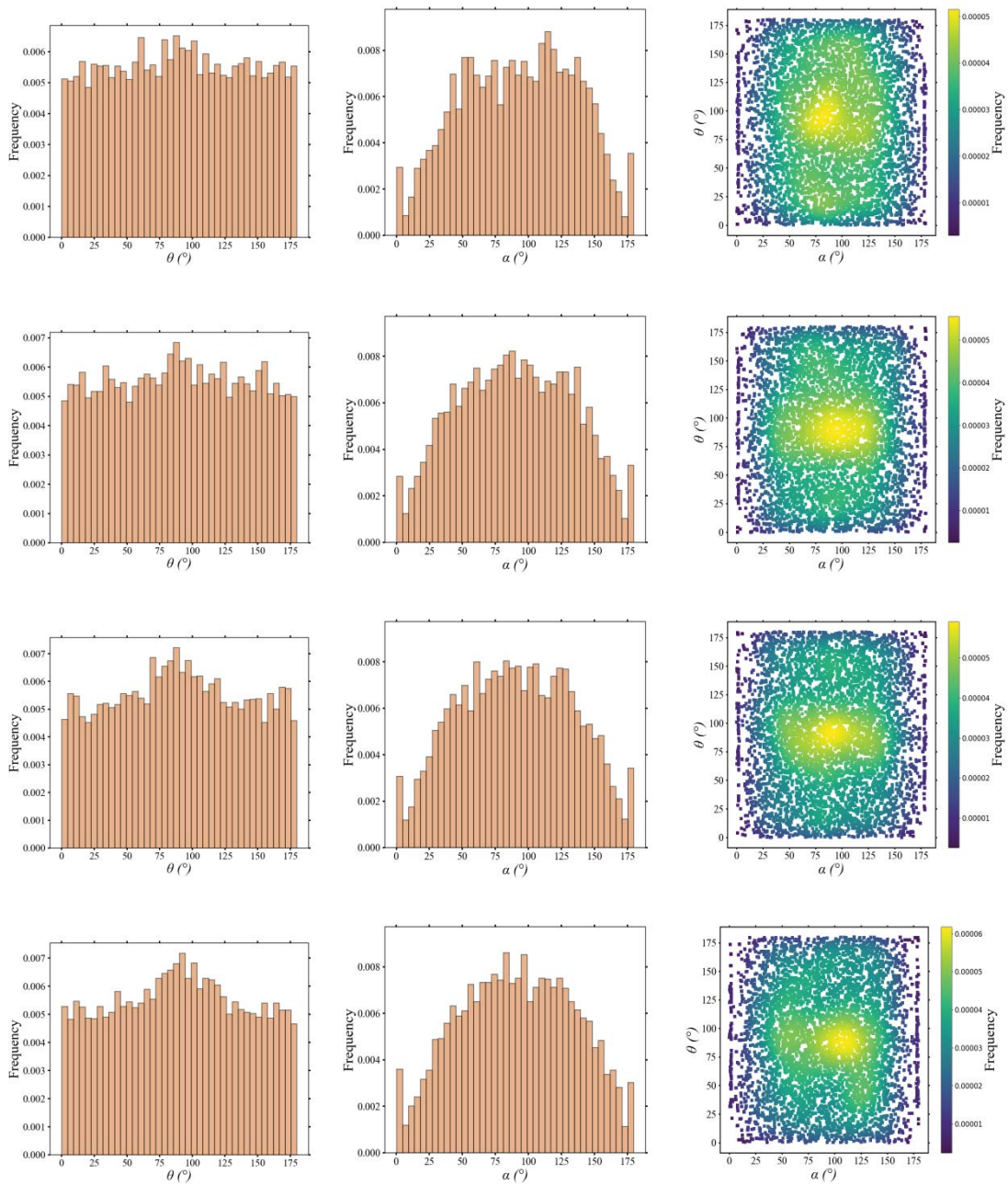
Fig. S8. The slits between CNTs is 1.3 nm, from top to bottom, each row corresponds to *r* = 0.5, 1.0, 2.0, and 3.0 nm, from left to right, each column corresponds to distribution of θ, distribution of *α*, bivariate joint distribution of θ and *α*.
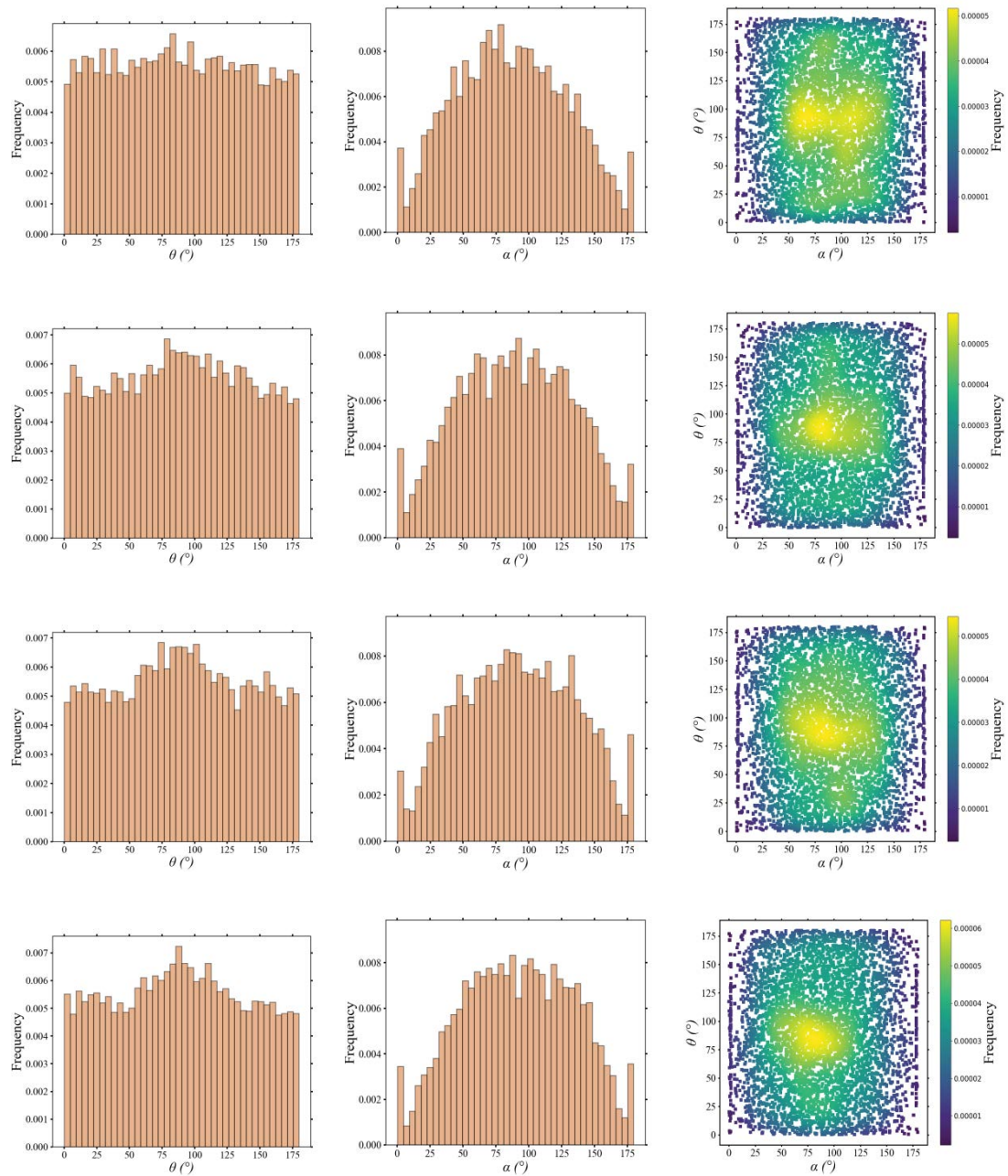
Fig. S9. The slits between CNTs is 1.5 nm, from top to bottom, each row corresponds to r = 0.5, 1.0, 2.0, and 3.0 nm, from left to right, each column corresponds to distribution of θ, distribution of α, bivariate joint distribution of θ and α.